Brain Pathology ISSN 1015-6305

RESEARCH ARTICLE

PET of Brain Prion Protein Amyloid in Gerstmann–Sträussler–Scheinker Disease

Vladimir Kepe[1]; Bernardino Ghetti[2]; Martin R. Farlow[2]; Mara Bresjanac[3]; Karen Miller[1]; Sung-Cheng Huang[1]; Koon-Pong Wong[1]; Jill R. Murrell[2]; Pedro Piccardo[2]; Francine Epperson[2]; Grega Repovš[4]; Lojze M. Smid[1,3]; Andrej Petrič[5]; Prabha Siddarth[1]; Jie Liu[1]; Nagichettiar Satyamurthy[1]; Gary W. Small[1]; Jorge R. Barrio[1]

[1] David Geffen School of Medicine at UCLA, Los Angeles, Calif.
[2] Indiana University School of Medicine, Indianapolis, Ind.
[3] Medical Faculty, [4] Faculty of Arts, [5] Faculty of Chemistry and Chemical Technology, University of Ljubljana, Ljubljana, Slovenia.

Keywords
amyloid, [F-18]FDDNP, [F-18]FDG, familial prion disease, GSS A117V, GSS F198S "Indiana kindred", GSS P102L, positron emission tomography, *PRNP* gene mutation, tau, transmissible spongiform encephalopathy.

Corresponding author:
Jorge R. Barrio, PhD, Department of Molecular and Medical Pharmacology, David Geffen School of Medicine at UCLA, Los Angeles, CA 90095-6948 (E-mail: *jbarrio@mednet.ucla.edu*)

Received 17 February 2009; accepted 27 April 2009.

Contributors: VK, BG, MRF, MB, S-CH, GWS and JRB participated in the design of the study. VK, BG, MRF, KM, FE, JL, NS, GWS and JRB were instrumental in performing the imaging study. VK, S-CH, KPW and JRB developed image analysis methodology and analyzed the imaging data. MB, GR, LMS and AP performed *in vitro* tissue labeling experiments and analysis. VK, BG, MRF, MG, KM, S-CH, JRM, PP, LMS, PS, GWS and JRB evaluated the data. VK, BG, MB and JRB contributed to the development of the first draft. VK and JRB developed the final draft. All authors contributed to the writing and the revision of this paper, and approved the final version.

doi:10.1111/j.1750-3639.2009.00306.x

Abstract

In vivo amyloid PET imaging was carried out on six symptomatic and asymptomatic carriers of *PRNP* mutations associated with the Gerstmann–Sträussler–Scheinker (GSS) disease, a rare familial neurodegenerative brain disorder demonstrating prion amyloid neuropathology, using 2-(1-{6-[(2-[F-18]fluoroethyl)(methyl)amino]-2-naphthyl}ethylidene)malononitrile ([F-18]FDDNP). 2-Deoxy-2-[F-18]fluoro-D-glucose PET ([F-18]FDG) and magnetic resonance imaging (MRI) scans were also performed in each subject.

Increased [F-18]FDDNP binding was detectable in cerebellum, neocortex and subcortical areas of all symptomatic gene carriers in close association with the experienced clinical symptoms. Parallel glucose metabolism ([F-18]FDG) reduction was observed in neocortex, basal ganglia and/or thalamus, which supports the close relationship between [F-18]FDDNP binding and neuronal dysfunction. Two asymptomatic gene carriers displayed no cortical [F-18]FDDNP binding, yet progressive [F-18]FDDNP retention in caudate nucleus and thalamus was seen at 1- and 2-year follow-up in the older asymptomatic subject. *In vitro* FDDNP labeling experiments on brain tissue specimens from deceased GSS subjects not participating in the *in vivo* studies indicated that *in vivo* accumulation of [F-18]FDDNP in subcortical structures, neocortices and cerebellum closely related to the distribution of prion protein pathology. These results demonstrate the feasibility of detecting prion protein accumulation in living patients with [F-18]FDDNP PET, and suggest an opportunity for its application to follow disease progression and monitor therapeutic interventions.

Abbreviations: GSS, Gerstmann–Sträussler–Scheinker disease; PrP, prion protein; *PRNP*, prion protein gene; PrP^{C}, normal cellular form of the prion protein; PrP^{Sc}, disease-specific isoform of the prion protein; CJD, Creutzfeldt–Jakob disease.

BACKGROUND

Human prion diseases or transmissible spongiform encephalopathies are a group of rare neurodegenerative disorders, which include sporadic, familial, iatrogenic and variant forms of Creutzfeldt–Jakob disease (CJD), Gerstmann–Sträussler–Scheinker disease (GSS), sporadic and familial fatal insomnia and kuru (3–5, 10, 11, 21, 25–27). Prion diseases are characterized by a wide spectrum of clinical abnormalities that include ataxia, myoclonus, pyramidal and extrapyramidal signs and cognitive impairment. The pathological hallmark of these diseases is accumulation of a pathological form of the prion protein (PrP), in some cases in the form of prion protein amyloid plaques in addition to spongiform changes (vacuolation), astrocytic proliferation and neuronal

loss, all of which can be found in patterns, varying by illness and disease stage, throughout the cerebrum, cerebellum and subcortical structures (4, 6, 8, 10, 28, 30).

Although the worldwide incidence of CJD is estimated as one case per million per year (27), the detection of transmissible spongiform encephalopathies in cattle in Great Britain in the 1980s demonstrated their potential for rapid spread to humans. As a result, the role of imaging modalities in their early detection is being investigated (33). In addition to FDDNP (2), two Congo red derivatives, methoxy-X04 (29) and (*trans*,*trans*)-1-bromo-2,5-bis-(3-hydroxycarbonyl-4-hydroxy)styrylbenzene (15), and a thioflavin derivative, 2-[4′-(methylamino)phenyl]benzothiazole (15) were initially suggested as potential imaging probes to target prion amyloid deposits *in vivo*. These probes have been reported to bind to compact PrP plaques in selected brain specimens of human prion diseases and mice infected with transmissible spongiform encephalopathy after intravenous injection, but their use in living humans has not yet been reported.

In this work, we investigated 2-(1-{6-[(2-[F-18]fluoroethyl)(methyl)amino]-2-naphthyl}ethylidene)malononitrile ([F-18]FDDNP) as a PET imaging ligand for prion diseases in the brain of six living subjects carrying mutations associated with GSS. The *in vivo* use of [F-18]FDDNP was supported by earlier *in vitro* experiments with human brain specimens from selected prion diseases and other neurodegenerative disorders (2, 32). To test the effectiveness of *in vivo* [F-18]FDDNP PET in visualizing PrP amyloid load, we chose subjects from three GSS families with known point mutations of the *PRNP* gene (Table 1). GSS mutation carriers with known pathologal characteristics (Supporting Data) were chosen to assess the sensitivity of the imaging tools and evaluate their limitations. GSS is a good disease model for these imaging studies because of its predictable clinical progression resulting from the high penetrance of the autosomal dominant mutations and because of high amyloid load. [F-18]FDDNP PET data were compared with 2-deoxy-2-[F-18]fluoro-D-glucose ([F-18]FDG) PET, as well as structural magnetic resonance imaging (MRI) brain scans on the same subjects and the results statistically correlated with their clinical symptoms and disease evolution. Twelve-, and 27- to 28-month follow-up data were obtained on two mutation carriers, respectively, one with the F198S mutation and the other with P102L mutation.

PATIENTS AND METHODS

All procedures were approved by the human subject protection committees of the University of California at Los Angeles and Indiana University. A written informed consent was obtained from all subjects or their legal representative if the subjects were cognitively impaired.

Participants

Six GSS subjects carrying *PRNP* gene point mutations participated in the study: one symptomatic P102L carrier (subject 10141, codon 129 M/M), one symptomatic A117V carrier (subject 10308, codon 129 V/V), two symptomatic F198S carriers (Indiana kindred, subject 10136, codon 129 V/V; and subject 10151, codon 129 V/V) and two asymptomatic (subject 10142, codon 129 M/V; and subject 10158, codon 129 M/V) (patient demographics in

Table 1. Demographic data for subjects participating in the study.

Subject (mutation)	Scan	Gender	Codon 129 status	Age*	Time after disease diagnosis (years)	MMSE* score	Neurological assessment*
10141 (P102L)	Baseline	M	M/M	43	1	26	Uncoordinated gait, myoclonic jerks, memory deficits
	12-month follow-up			44	2	27	Increased motor incoordination, mild bradykinesia
	27-month follow-up			46	4	28	Severe deterioration Decreased gaited stability, tremor in all extremities, progressive cognitive impairment
10308 (A117V)	Baseline	M	V/V	45	2	18	Dementia, ataxia, Parkinsonism, depression, generalized weakness
10136 (F198S)	Baseline	F	V/V	39	3	23	Parkinsonian symptoms, motor incoordination, depression, cerebellar dysfunction and cognitive deficits. Wheel-chair bound
10151 (F198S)	Baseline	M	V/V	48	3	24	Parkinsonian symptoms, dystaxia, motor incoordination, dementia
10142 (F198S)	Baseline	F	M/V	44	—	30	Asymptomatic
	12-month follow-up			45	—	30	Asymptomatic
	28-month follow-up			47	—	30	Asymptomatic
10158 (F198S)	Baseline	F	M/V	30	—	28	Asymptomatic
Alzheimer's disease	—	5F/5M	—	72.2 ±6.6	—	18.4 ±3.3	—
Controls	—	6F/4M	—	43.8 ±6.9	—	29.8 ±0.4	—

*At the time of the PET/MRI scans. Group values are given as mean ± 1 SD.

Table 1). The subjects were recruited from the cohort of PrP-mutation-carrier subjects, clinically evaluated (Martin R. Farlow, MD) at the Indiana Alzheimer Disease Center, Indiana University, to participate in a large PET imaging study of Alzheimer's disease (AD) and other dementias conducted at the University of California at Los Angeles. Ten age-matched, cognitively normal control subjects (six females, four males; average age: 43.8 ± 6.9, ranging from 30 to 52 years) and 10 subjects with mild to moderate AD (five females, five males; average age: 72.2 ± 6.6) were used for comparison.

All GSS subjects received clinical and neuropsychological evaluations at the Indiana Alzheimer Disease Center, and were reevaluated on a yearly basis when possible. Initial diagnoses and change in disease status were determined at consensus diagnostic conferences. Each subject also underwent additional neuropsychological testing (18) at UCLA each time they received [F-18]FDDNP, [F-18]FDG-PET and MRI scans (full clinical and cognitive profiles included in Supporting Tables S3 and S4).

Imaging protocols

MRI

T1-weighted magnetization prepared rapid acquisition gradient echo (MPRAGE) MRI volumetric scans, using a 3T Siemens Allegra MRI scanner (Erlangen, Germany) (sagittal plane; repetition time 2300 ms; echo time 2.93 ms; 160 slices; slice thickness 1 mm, skip 0.5 mm; in-plane voxel size 1.3 × 1.3 mm; field of view 256 × 256; flip angle 8°), were obtained.

Imaging protocols

PET

PET scans were performed sequentially at the UCLA Ahmanson Biomedical Imaging Center using a Siemens CTI ECAT HR+ scanner (Knoxville, TN) within 3 days after each MRI scan. After 10 minutes attenuation scan on the patient lying in a supine position on the tomograph bed, scanning was initiated following a bolus intravenous injection of either 10 mCi (370 MBq) of [F-18]FDDNP (19) or [F-18]FDG (24). Dynamic acquisition frames were obtained as follows; for [F-18]FDDNP: 6 × 30 s, 4 × 180 s, 5 × 600 s and 3 × 1200 s for the total duration of 2 h; for [F-18]FDG PET: 9 × 5 s, 3 × 15 s, 3 × 30 s, 1 × 120 s, 5 × 300 s and 3 × 600 s for the total duration of 1 h. All scans were corrected for decay and reconstructed using filtered back-projection (Hann filter, 5.5 mm FWHM) with scatter correction and measured attenuation correction. The resulting images contained 63 contiguous slices with the plane-to-plane separation of 2.42 mm. No partial volume correction was performed.

Imaging analysis: Logan graphical analysis of [F-18]FDDNP data

Parametric images of relative distribution volume (DVR) (16, 31) were generated by Logan graphical analysis, using the time–activity curve of white matter as the reference (20) as previously described (11). In these cases, reference region-of-interest (ROI) placement is on large volume of white matter in the frontal lobe. [F-18]FDDNP DVR parametric images, generated using dynamic frames between 25 minutes and 65 minutes, were analyzed using ROIs drawn on co-registered MRI for left and right parietal, medial temporal (limbic regions, including the hippocampus, parahippocampal areas and entorhinal cortex), lateral temporal, posterior cingulate and frontal regions (31). The average of all cortical regional values was used as a measure of global cortical DVR. Use of white matter as a reference region was validated by comparing results of [F-18]FDDNP PET data from 10 controls and 10 AD patients using Logan graphical analysis with cerebellum (31) and white matter as reference regions (37) (Supporting Figure S1). [F-18]FDDNP R1 values, defined as the ratio of brain delivery from blood to brain tissue in the target tissue (Ki) and the reference tissue (K1R; white matter), were obtained as previously described (37).

[F-18]FDG SUVR values

[F-18]FDG PET images, containing summed data from 30 minutes to 60 minutes, were analyzed using a set of ROIs drawn bilaterally on frontal, parietal, lateral temporal, medial temporal cortices, posterior cingulate gyrus (31) and on striatum, thalamus and cerebellar cortex. SUVR was calculated as the ratio of the ROI value in the area of interest to the ROI value on the white matter (23). The average of all cortical regional values was used as a measure of global cortical SUVR. As cortical coincidence of pathological deposition of amyloid with glucose metabolic deficits is not necessarily expected, two separate sets of ROIs were used for [F-18]FDDNP and [F-18]FDG (16, 31).

FDDNP fluorescence microscopy and immunohistochemistry to tau and PrP

All subjects studied remained alive at the time this work was completed. Thus, confirmatory FDDNP (2, 32) labeling experiments were performed on brain tissue specimens from 11 deceased members of the Indiana GSS kindred not participating in the imaging experiments, including one mutation carrier who died before the onset of clinical symptoms. Brain sections from a person with no neurological disorder were used as negative controls (detailed description of methods in Supporting Methods).

RESULTS

[F-18]FDDNP PET

Summary results are provided in Table 2, and representative scans are provided in Figures 1 and 2. All symptomatic subjects showed elevated subcortical [F-18]FDDNP binding consistent with extended distribution of pathology in basal ganglia and thalamus (9), and also consistent with the observed clinical symptoms attributable to impairment in subcortical structures most characteristically extrapyramidal symptoms. In all severe symptomatic cases, global cortical and subcortical (ie, basal ganglia and thalamus) hypometabolism, as well as severe atrophy, were prominently present (Figures 1 and 3A,B,G; Table 3; MRI images Supporting Figure S2).

All symptomatic subjects, with the exception of subject 10308 (A117V mutation carrier), also demonstrated increased

Table 2. [F-18]FDDNP DVR values for Gerstmann–Sträussler–Scheinker subjects. Abbreviations: S = symptomatic; A = asymptomatic.

Subject	Scan	Status	DVR								
			Cerebellum	Striatum	Thalamus	Frontal	Parietal	Medial temporal	Lateral temporal	Posterior cingulate	Global
10141 (P102L)	Baseline	S	**1.036***	**1.314***	**1.361***	1.052	1.024	1.111	**1.163**	1.064	**1.083***
	12-month follow-up	S	**1.051***	**1.449***	**1.418***	**1.106**	**1.095**	1.145	**1.159**	1.113	**1.124***
	27-month follow-up	S	**1.044***	**1.51***	**1.44***	**1.16**	**1.087**	**1.178**	**1.16**	**1.176**	**1.152***
10308 (A117V)	Baseline	S	0.984	**1.61**	**1.5**	**1.191**	**1.296**	1.134	**1.204**	**1.184**	**1.202**
10136 (F198S)	Baseline	S	**1.06**	**1.519**	**1.316**	1.057	**1.117**	1.097	1.108	1.122	**1.1**
10151 (F198S)	Baseline	S	**1.109**	**1.631**	**1.721**	1.07	**1.086**	1.144	**1.13**	1.113	**1.109**
10142 (F198S)	Baseline	A	0.991*	**1.375***	1.244*	1.058	**1.075**	1.108	1.069	1.081	1.078*
	12-month follow-up	A	0.998*	**1.389***	**1.291***	1.064	**1.09**	1.144	1.106	1.088	**1.098***
	28-month follow-up	A	0.994*	**1.436***	**1.342***	1.054	**1.072**	**1.167**	1.084	1.059	**1.087***
10158 (F198S)	Baseline	A	0.989	1.166	1.124	0.965	1.01	1.117	1.061	1.04	1.039
Alzheimer's disease	—	—	0.998	1.265†	1.233	1.064	1.132†	1.175†	1.15†	1.177†	1.14†
(10 subjects)			±0.015	±0.090	±0.082	±0.043	±0.036	±0.034	±0.027	±0.033	±0.011
Controls	—	—	0.989	1.178	1.164	1.01	1.03	1.096	1.051	1.061	1.05
(10 subjects)			±0.019	±0.036	±0.052	±0.034	±0.018	±0.034	±0.030	±0.039	±0.016

DVR values were determined with Logan graphical analysis using white matter as reference region. Cumulative data for 10 age-matched controls and 10 Alzheimer's disease patients are shown for comparison.
[F-18]FDDNP DVR values shown in bold and underlined are 2 SD higher than the mean value for the same brain regions in the control group. Group values are given as mean ± 1SD.
*Indicated values are shown in graphical form in Supporting Figure S3.
†Indicated mean AD group values are 2 SD higher than the mean value for the control group in the same brain regions.

Table 3. [F-18]FDG SUVR values for Gerstmann–Sträussler–Scheinker subjects. Abbreviations: S = symptomatic; A = asymptomatic.

Subject	Scan	Status	SUVR									
			Cerebellum	Striatum	Thalamus	Frontal	Parietal	Medial temporal	Lateral temporal	Posterior cingulate	Global	Motor cortex
10141 (P102L)	Baseline	S	**1.246**	**1.478***	**1.504***	**1.572**	**1.311**	1.345	**1.267**	**1.579**	**1.415***	**1.79**
	12-month follow-up	S	**1.196**	**1.508***	**1.44***	**1.404**	**1.307**	1.263	**1.151**	**1.612**	**1.347***	**1.747**
	27-month follow-up	S	**1.157**	**1.475***	**1.336***	**1.451**	**1.093**	1.269	**1.088**	**1.565**	**1.293***	**1.711**
10308 (A117V)	Baseline	S	1.435	**1.243**	**1.252**	**1.459**	**1.221**	**1.169**	**1.326**	**1.302**	**1.295**	**1.578**
10136 (F198S)	Baseline	S	1.382	**1.247**	**1.572**	**1.561**	**1.194**	1.345	**1.268**	**1.532**	**1.38**	**1.793**
10151 (F198S)	Baseline	S	**1.004**	**1.586**	**1.277**	**1.574**	**1.454**	1.388	1.511	**1.152**	**1.16**	**1.755**
10142 (F198S)	Baseline	A	1.427	**1.663***	1.666*	1.67	**1.455**	1.52	**1.416**	1.898	1.592*	1.999
	12-month follow-up	A	1.285	**1.698***	1.692*	1.736	**1.502**	1.289	1.503	2.035	1.613*	1.953
	28-month follow-up	A	1.384	**1.675***	1.693*	1.644	**1.495**	1.436	1.483	1.907	1.593*	1.92
10158 (F198S)	Baseline	A	1.443	1.923	1.878	1.831	1.689	1.421	1.547	1.992	1.696	1.914
Alzheimer's disease	—	—	1.605	1.957	1.855	1.472†	1.224†	1.131†	1.249†	1.67†	1.322†	1.91
(10 subjects)			±0.113	±0.125	±0.189	±0.158	±0.185	±0.095	±0.231	±0.175	±0.169	±0.067
Controls	—	—	1.584	1.953	1.867	1.771	1.848	1.351	1.605	2.06	1.727	1.957
(10 subjects)			±0.158	±0.086	±0.133	±0.063	±0.126	±0.083	±0.061	±0.089	±0.084	±0.054

SUVR values were also normalized to white matter. Cumulative data for 10 age-matched controls and 10 Alzheimer's disease patients are shown for comparison.
[F-18]FDG SUVR values shown in bold and underlined are 2 SD lower than the mean value for the same brain regions for the control group. Group values are given as means ± 1 SD. Normalization to white matter (16) was used instead of normalization to motor cortex (18) because of involvement of motor cortex in the disease (see motor cortex SUVR).
*Indicated values are shown in graphical forms in Supporting Figure S3.
†Indicated mean AD group values are 2 SD lower than the mean value for the control group in the same brain regions.

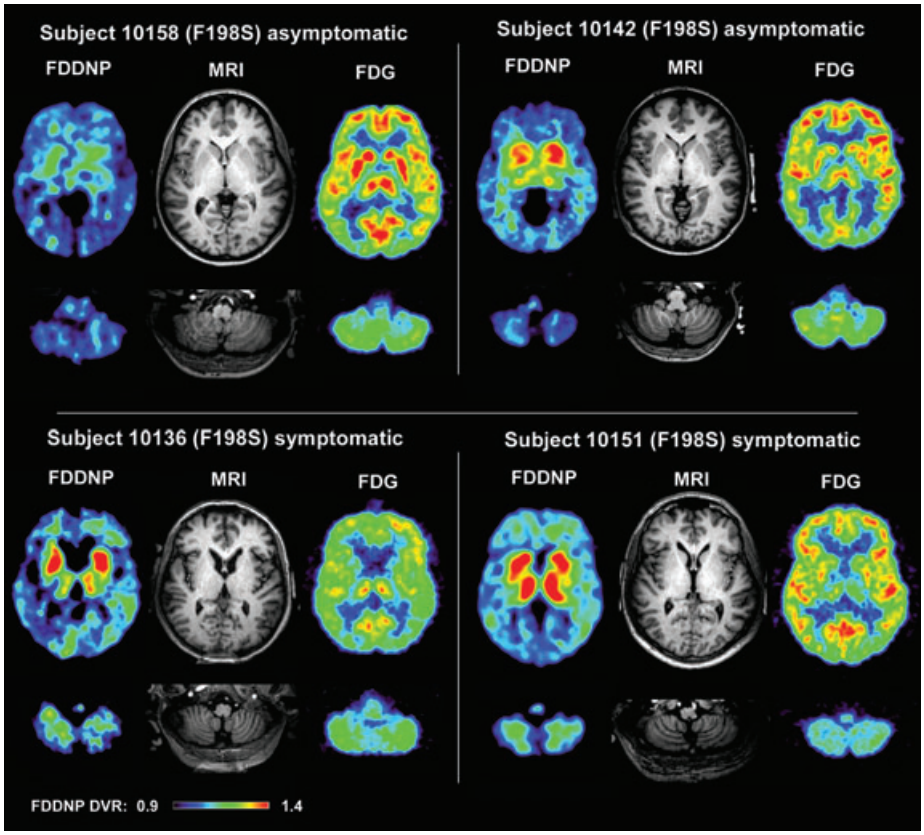

Figure 1. *[F-18]FDDNP PET, MRI and [F-18]FDG PET imaging results for four carriers of F198S mutation.* [F-18]FDDNP, [F-18]FDG and MRI scans in the asymptomatic subject 10158 are comparable with those of the age-matched control group. By contrast, asymptomatic subject 10142 shows increased [F-18]FDDNP binding and mildly decreased [F-18]FDG uptake in basal ganglia. Both symptomatic subjects 10136 and 10151 have increased [F-18]FDDNP binding in basal ganglia and thalamus, which is paralleled by decreases in [F-18]FDG uptake in the same areas. Consistent with pathology reports on presence of prion protein plaques in cerebellum, both subjects have increased [F-18]FDDNP binding in the cerebellum. Cerebral cortex is affected to various degrees with variable patterns of binding. Warmer color images represent higher uptake.

[F-18]FDDNP binding in cerebellum, as expected from the known distribution of GSS pathology in advanced stages (10). This accumulation is entirely consistent with the progressive development of incoordination, decreased gait stability, dystaxia and other cerebellar dysfunction in these patients. The absence of cerebellar [F-18]FDDNP binding in the A117V mutation carrier is consistent with the small amount of PrP amyloid plaques in the cerebellum associated with this mutation (eg, subject 10308 is a telencephalic variant of A117V GSS based on clinical and MRI results) (10, 13) (Figure 2C).

All symptomatic subjects showed increased levels of global cortical [F-18]FDDNP binding compared with the normal control subjects with distribution patterns that differed among cases (Figure 3C–E). Regional subcortical and cortical differential [F-18]FDDNP patterns, as well as their evolution in patient follow-up, are the best parameters to determine differences in [F-18]FDDNP accumulation patterns (31) as done in this work. To establish diagnostic sensitivity and specificity of [F-18]FDDNP for GSS vs. AD, a larger number of cases would be required. One asymptomatic gene carrier (10158; GSS F198S mutation) showed minimal [F-18]FDDNP cerebral binding, comparable with that of control subjects. The other asymptomatic subject (10142, GSS F198S mutation) demonstrated increased bilateral [F-18]FDDNP binding (>2 SD) in the caudate nucleus with incipient cortical involvement at the time of the first scan. Interestingly, in spite of the lack of clinical symptoms, glucose metabolic deficits in basal ganglia (>2 SD) and thalamus (>1 SD) were also present (Figures 2B and 3A,B).

Longitudinal follow-up of subjects

Two patients received follow-up scans (Table 2; Figure 2A,B). For symptomatic subject 10141 (P102L GSS), the initial [F-18]FDDNP scan showed increased binding in the basal ganglia and thalamus, which steadily increased in repeated follow-up scans at 12 months and 27 months after the initial scan (Figure 3C–E; see also Supporting Figure S3 and Supporting Table S1). Cerebellar [F-18]FDDNP binding was increased in all three scans with no

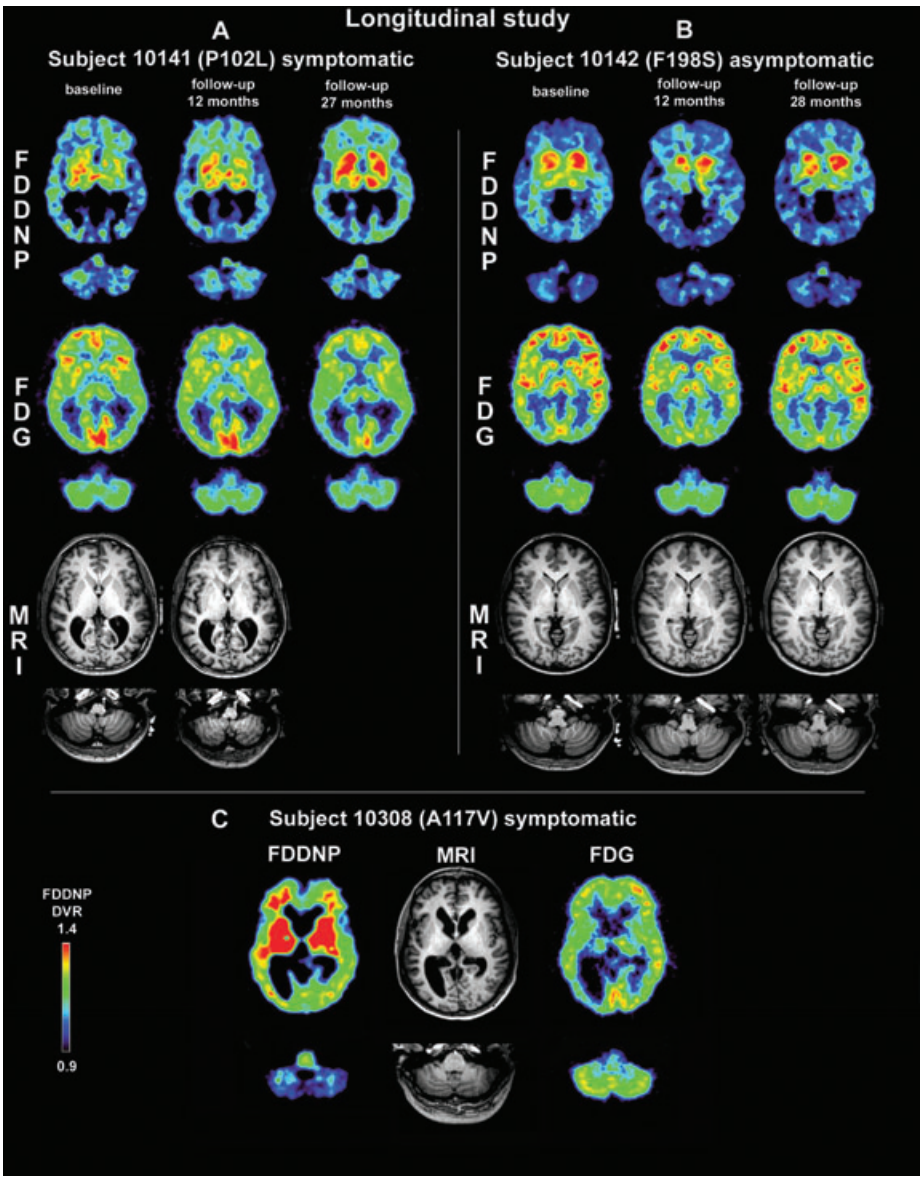

Figure 2. *[F-18]FDDNP PET, MRI and [F-18]FDG PET imaging results of longitudinal study of symptomatic P102L mutation carrier 10141 (A) and asymptomatic F198S mutation carrier 10142 (B), and imaging results for PRNP mutations A117V carrier 10308 (C).* (**A**) Imaging results of the three-point 27-month longitudinal study of P102L mutation carrier 10141 from early symptomatic stage (baseline) to very affected stage (27-month follow-up). Cerebellum shows increased levels of [F-18]FDDNP binding at all three stages; basal ganglia, thalamus and cerebral cortex show increased levels of binding at both follow-up points. [F-18]FDG also demonstrates progressive decline, most notably in basal ganglia and parieto-temporal areas. (**B**) Results of the three-time point 28-month longitudinal study in asymptomatic F198S subject 10142. [F-18]FDDNP demonstrates progressive involvement of basal ganglia and thalamus, paralleled by metabolic deficits ([F-18]FDG) in similar areas. (**C**) Imaging results for the symptomatic A117V mutation carrier 10308. The brain is heavily affected as reflected in severe loss of white matter, cortical atrophy and enlargement of all ventricles (MRI). High [F-18]FDDNP binding was observed in all cortical and subcortical areas with exception of cerebellum which shows no signal above control levels. This is paralleled by [F-18]FDG uptake decrease in whole brain with the exception of cerebellum. Warmer colors represent higher uptake.

apparent progression. The cerebral cortex showed the most prominent binding in the lateral temporal lobe at baseline, and this lateral temporal cortical binding increased and extended to the parietal cortex and posterior cingulate gyrus at follow-up.

The patterns of progression in follow-up scans were consistent with progressive neurological and neuropsychological decline observed on clinical examination, which included severe general neurological deterioration with increased cerebellar

incoordination and decreased gait stability. T1 MRI scans available at baseline and 12-month follow-up showed dilated lateral ventricles and global cortical atrophy, which progressed at follow-up. The [F-18]FDG PET scans showed reduced uptake in basal ganglia, thalamus and all cortical regions at baseline, and further decline in glucose utilization at two follow-up scans (12 months and 27 months), most prominently in the parietal regions, all of which are also consistent with the progressive cognitive deterioration observed in this patient (Figures 2A and 3F,G; see also Supporting Tables S3 and S4).

Asymptomatic subject 10142 (F198S GSS) also had three [F-18]FDDNP scans (baseline, 12-month and 28-month follow-up). Interestingly, [F-18]FDDNP binding in basal ganglia and thalamus, with sparing of most cortical areas and cerebellum, was observed at baseline and at follow-up. [F-18]FDG PET showed minimal glucose metabolic decline in subcortical and parietal regions, all of which suggest the subcortical nature of initial prion deposition (Table 3; see also Supporting Figure S4 and Supporting Table S2). T1 MRI scans at follow-up were comparable with those of controls with no noticeable atrophy or ventricular dilation. Even though no abnormal clinical signs were manifested in this subject, the results of cognitive tests pointed to subtle deterioration in at least one cognitive domain (ie, verbal and visual memory tasks) (Supporting Table S4). Perfusion delivery in subcortical structures—the brain areas with higher [F-18]FDDNP DVR in the GSS subjects studied in this work—is not significantly affected, regardless of the degree of disease severity (R1 values, see Supporting Figure S5).

In vitro fluorescent FDDNP labeling of GSS brain specimens

In vitro labeling determinations carried out on brain sections of F198S GSS cases confirmed FDDNP's ability to bind strongly to prion plaques with dense cores, and moderately labeled diffuse plaques, in the cerebral and cerebellar cortex and the striatum (Figure 4, panel 1a–f) (2, 32). Only background signal was observed in control brain sections (Figure 4, panel 1g–i). A co-localization analysis of FDDNP fluorescence with prion or tau immunoreactivity showed that on average, 89% of the area labeled by FDDNP was also immunoreactive to prion-specific antibody (Figure 4, panel 2a–c), with an average co-localization coefficient M_{FDDNP} of 0.91. By contrast, in the case of tau aggregates, only 33% of the area labeled by FDDNP was also labeled by tau IHC (Figure 4, panel 2d–f) with the average co-localization coefficient M_{FDDNP} of 0.17. Two-tailed Wilcoxon rank sum test showed the differences in both measures (percent of signal area overlap and the co-localization coefficient) between FDDNP–prion IHC and FDDNP–tau IHC to be highly significant ($W = 0$, $P = 0.00001$).

DISCUSSION

This investigation demonstrates that [F-18]FDDNP brain binding patterns in patients with GSS and asymptomatic gene carriers follow the distribution and progression of PrP deposition expected in living people with GSS-associated mutations, and is also in consistent agreement with clinical symptoms. [F-18]FDDNP scans of the confirmed F198S mutation carriers—at various clinical stages of the illness—provide the first glimpse into the pathology development in the living brain of these subjects. In two asymptomatic F198S mutation carriers studied, [F-18]FDDNP scans were either similar to controls (10158), or showed increased binding in subcortical structures and limited cortical involvement (10142) (Figure 1) in patterns comparable with those observed in familial AD gene mutation carriers (17). Detectable progression of [F-18]FDDNP accumulation in asymptomatic F198S GSS subject 10142, accompanied with hypometabolism in the same cortical and subcortical structures (Tables 2 and 3; Figure 3A,B) is indicative of the clinically silent evolution of the disease and the compensatory mechanisms at play to preserve function, as earlier observed with [F-18]FDG PET in asymptomatic at-risk Huntington's disease mutation carriers (22).

The increased [F-18]FDDNP binding in subcortical and cortical structures, including the cerebellum, observed in symptomatic F198S GSS patients (10136 and 10151) likely reflects more extended disease-related brain damage. At this stage, widespread cortical and subcortical brain damage is responsible for the prominent neuropsychiatric and motor symptoms observed, including ataxia, Parkinsonian signs and progressive cognitive decline (7, 9). These [F-18]FDDNP PET results are also consistent with the localization of PrP deposition characteristically found at autopsy in this disease (10). In advanced stages, damage to neuronal circuits is widespread as reflected in the observed decreased metabolism in [F-18]FDG scans of GSS mutations carriers (12, 34). MRI results are also in agreement with earlier observations that structural MRI often appears normal in Creutzfeldt–Jakob disease and GSS at the onset of the disease, yet atrophy is a prominent feature in sequential follow-up scans reflecting disease progression (14, 35).

In vitro analysis of fluorescent FDDNP labeling in brain sections of GSS patients supports the *in vivo* [F-18]FDDNP PET findings. The moderately FDDNP-labeled loose-structured prion plaques present in great abundance in the striatum and thalamus (9) are the most likely source of the high [F-18]FDDNP PET binding observed in these regions in the living brain of F198S GSS subjects. Co-localization analysis (of fluorescent FDDNP and IHC labeling) indicated that FDDNP targets primarily PrP deposits and not the tau aggregates which are widely present in the brains of F198S mutation subjects. Nevertheless, this analysis does not provide unequivocal evidence that prion amyloid is primarily labeled. To minimize confounding factors regarding the ability of [F-18]FDDNP to visualize prion accumulation in these patients, we incorporated a GSS symptomatic patient with a P102L mutation (10141) in this investigation. The clinical phenotype for this mutation is a progressive cerebellar syndrome presenting with either typical GSS or a combination of GSS and Creutzfeldt–Jakob disease neuropathological features (amyloid plaques and spongiform degeneration, but no appreciable tau pathology) (10, 36). In this P102L mutation carrier, the [F-18]FDDNP PET signal in the cerebellum, basal ganglia, thalamus and temporal lobe was found to be comparable with that in symptomatic F198S mutation subjects, wherein the cortical tau deposition is common. Based on the known distribution of PrP pathology in P102L patients, accumulation of [F-18]FDDNP in the neocortex and cerebellum is expected, as well as involvement of the medial temporal lobe, which is consistent with the

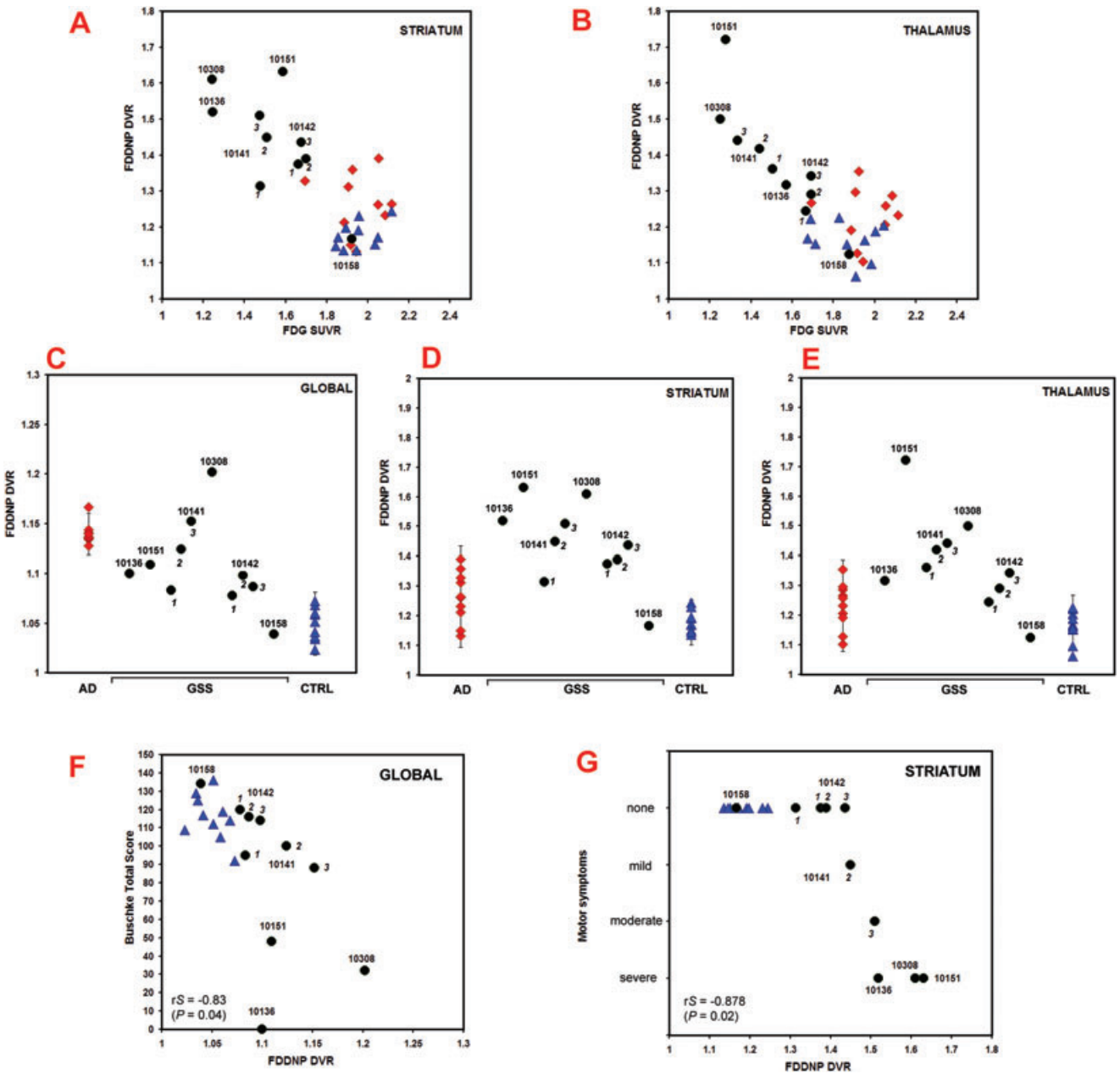

commonly observed memory and other psychomotor deficits. Progressive ataxia in subject 10141 was also correlated with increases in [F-18]FDDNP cortical and subcortical PrP deposition as shown in the 28-month follow-up of this patient (Figures 2A and 3F,G). Neuronal losses and circuit dysfunction resulting from spongiform degeneration and PrP plaques are also suggested by widespread progression of global hypometabolism, and evidenced clinically by generalized deterioration of motor and neuropsychiatric function (Table 2; Figure 3A,B,F,G) (34).

These [F-18]FDDNP PET observations, taken together with the *in vitro* results, suggest that prion plaque labeling alone accounts for the most prominent portion of the signal observed in F198S GSS subjects. To further demonstrate the discriminative value of [F-18]FDDNP PET in assessing prion aggregate deposition in the brain of GSS patients, we incorporated to this investigation a patient from an A117V family (10308). In this mutation, variable amounts of PrP amyloid plaques and diffuse deposits are found in cerebral cortex, hippocampus, basal ganglia and thalamus, but they may be absent or present in small amounts in the cerebellum (10). In agreement with these pathological observations, [F-18]FDDNP PET binding in this patient (10308) demonstrates relative sparing of cerebellum, but widespread cortical and subcortical involvement consistent with their clinical symptoms.

Figure 3. (**A,B**) Correlation of [F-18]FDDNP DVR and [F-18]FDG SUVR in striatum and thalamus of Gerstmann–Sträussler–Scheinker (GSS) subjects (black symbols) in comparison with normal controls (blue symbols), and Alzheimer's disease patients (red symbols). (**C–E**) Scatter plots of [F-18]FDDNP DVR in striatum, thalamus and global cortices in the same GSS subjects. (**F,G**) Three-dimensional plots of [F-18]FDDNP DVR and [F-18]FDG SUVR global cortices vs. memory measures (Buschke total), and striatum vs. motor symptoms (rated as normal, mild, moderate and severe). Statistics: Spearman rank correlations of [F-18]FDDNP DVR values with [F-18]FDG SUVR values in striatum (**A**) and thalamus (**B**) were significant at $r_S = -0.497$ ($P = 0.05$) for striatum, and $r_S = -0.703$ ($P = 0.002$) for thalamus. (**C**) *Z* scores (number of SDs from control group mean value) for global [F-18]FDDNP DVR are: symptomatic subject 10136 = 3.1; symptomatic subject 10151 = 3.7; symptomatic subject 10141 = 2.1, 4.6 and 6.4 for scans 1, 2 and 3, respectively; symptomatic subject 10308 = 9.5; asymptomatic subject 10142 = 1.8, 3.0 and 2.3 for scans 1, 2 and 3, respectively; asymptomatic subject 10158 = –0.7. (**D**) *Z* scores for striatum [F-18]FDDNP DVR are: symptomatic subject 10136 = 9.5; symptomatic subject 10151 = 12.6; symptomatic subject 10141 = 3.8, 7.5 and 9.2 for scans 1, 2 and 3, respectively; symptomatic subject 10308 = 12.0; asymptomatic subject 10142 = 5.5, 5.9 and 7.2 for scans 1, 2 and 3, respectively; asymptomatic subject 10158 = –0.3. (**E**) *Z* scores for thalamus [F-18]FDDNP DVR are: symptomatic subject 10136 = 2.9; symptomatic subject 10151 = 10.7; symptomatic subject 10141 = 3.8, 4.9 and 5.3 for scans 1, 2 and 3, respectively; subject 10308 = 6.5; asymptomatic subject 10142 = 1.5, 2.4 and 3.4 for scans 1, 2 and 3, respectively; asymptomatic subject 10158 is –0.8. (**F**) The following statistical correlations are observed: [F-18]FDG SUVR (global) vs. [F-18]FDDNP DVR (global) is significant with Spearman coefficient $r_S = -0.803$ ($P < 0.001$); [F-18]FDDNP DVR (global) vs. Buschke total significant with Spearman coefficient $r_S = -0.83$ ($P = 0.04$); and [F-18]FDG SUVR (global) vs. Buschke total significant with Spearman coefficient $r_S = 0.89$ ($P = 0.02$). (**G**) The following correlations are observed: [F-18]FDG SUVR (striatum) vs. [F-18]FDDNP DVR (striatum) is significant with Spearman coefficient $r_S = -0.497$ ($P < 0.05$); [F-18]FDDNP DVR vs. motor symptoms is significant with Spearman coefficient $r_S = -0.878$ ($P = 0.02$); and [F-18]FDG SUVR vs. motor symptoms was not significant with Spearman coefficient $r_S = 0.683$ ($P = 0.13$). *Z* scores for [F-18]FDDNP DVR and [F-18]FDG SUVR are included in Supporting Table S3 for all cortical and subcortical structures analyzed. Values larger than 2.0 SD are bolded.

This advanced A117V GSS patient showed severe intellectual decline and rigidity, major brain atrophy and prominent, generalized glucose metabolic deficits throughout the brain (Figure 2C).

In conclusion, the described results with [F-18]FDDNP PET applied to subjects with three GSS mutations are encouraging in their consistent relationship to the underlying neuropathology and the clinical presentation of the disease. These results confirm findings of an isolated [F-18]FDDNP PET study in a single patient from a family with 6-octapeptide repeat insertional *PRNP* mutation (1). Correlative assessment of local rates of glucose metabolism provides strong evidence of the relationship between PrP deposition and neuronal circuit dysfunction in cortical and subcortical structures. As a noninvasive *in vivo* method for prion plaque detection and quantification, [F-18]FDDNP PET also shows consistent appropriate increases associated with disease progression in two GSS subjects included in the follow-up study. These promising feasibility results suggest that [F-18]FDDNP PET may be a useful adjunct for confirmation of GSS. Of greater interest and potential clinical utility is the ability of [F-18]FDDNP PET to quantify changes in brain amyloid, and to assist the development of future therapies that may slow or halt disease progression. Further, the ability to demonstrate labeling associated with amyloid deposition prior to onset of clinical symptoms may in the future facilitate the development and application of putative treatments where the prion disease process may be more amenable to therapy. Studies in non-familial prion disease patients are needed before potential clinical utility in these populations can be determined.

ACKNOWLEDGMENTS

This work was supported by grants from DOE (DE-FC03-87-ER60615), NIH (P01-AG024831 and P30-AG10133) and ARRS P3-0171. Special thanks are given to Professor Stanley B. Prusiner, MD (University of California at San Francisco) for insightful comments and suggestions. PP is a current Food and Drug Administration (FDA) employee; the findings and conclusions in this article have not been formally disseminated by the FDA and should not be construed to represent any agency determination or policy. JRB gratefully acknowledges the support of the Elizabeth and Thomas Chair Endowment in Gerontology.

COMPETING INTERESTS STATEMENT

The authors declare competing financial interests. The University of California at Los Angeles owns a US patent (6 274 119) entitled "Methods for Labeling β-Amyloid Plaques and Neurofibrillary Tangles," that uses [F-18]FDDNP-PET and has been licensed to Siemens. GWS, S-CH, NS, AP and JRB are among the inventors, have received royalties and will receive royalties on future sales. GWS reports having served as a consultant and/or having received lecture fees from Abbott, Dakim, Eisai, Forest, Myriad Genetics, Novartis, Ortho-McNeil, Pfizer, Radica and Siemens. GWS also reports having received stock options from Dakim. S-CH reports having received lecture fees from GlaxoSmithKline. NS reports having served as a consultant for PETNET Pharmaceuticals and Siemens. MRF reports serving as a consultant for Adamas, Accera, Adlyfe, AstraZeneca, Astellas, Bristol-Myers Squibb, CoMentis, Eisai, Eli Lilly, GlaxoSmithKline, Medivation, Merck, Novartis, Noven, Octapharma, QR Pharma, Sanofi-Aventis and Toyama; is on Speaker Bureau for Eisai, Forest, Pfizer and Novartis; and receives research support from Bristol-Myers Squibb, Elan, Eli Lilly, Pfizer, Novartis, Octapharma and Sonexa. JRB reports having served as a consultant and having received lecture fees from Nihon Medi-Physics Co, Bristol-Myers Squibb, PETNET Pharmaceuticals and Siemens.

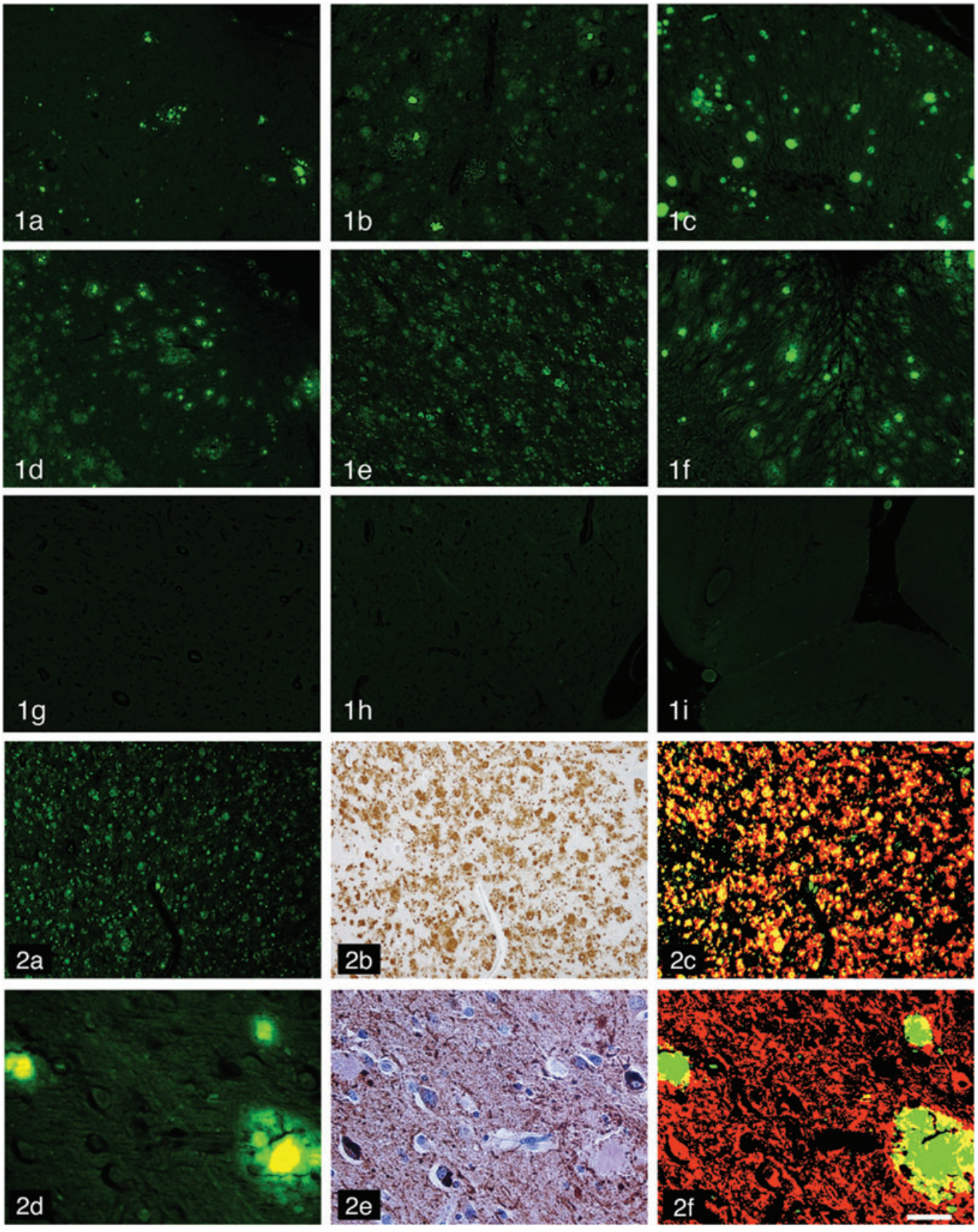

Figure 4. *Results of* in vitro *FDDNP fluorescence microscopy studies and immunohistochemical labeling of prion protein (PrP) and tau pathology in brain samples from F198S mutation Gerstmann–Sträussler–Scheinker (GSS) patients.* Panel 1a–i shows FDDNP fluorescent labeling (green signal) of the cerebral cortex (1a, 1d, 1g), striatum (1b, 1e, 1h) and cerebellum (1c, 1f, 1i) for the presymptomatic F198S mutation carrier (1a–1c), symptomatic GSS patient with the same mutation (1d–1f) and a normal control case (1g–1i). Intensely FDDNP fluorescent plaques with dense cores are present in all regions, but are particularly abundant in the cerebral and cerebellar cortex of both cases to a similar degree. The distinguishing feature between the GSS cases, also absent from the control brain, is the quantity of moderately labeled diffuse plaques lacking amyloid core: they are more abundant in all three regions of the symptomatic case (1d–1f). Panel 2a–c shows striatal labeling with FDDNP (green in 2a); IHC to prion protein (brown in 2b); and superimposed images of both signals, showing FDDNP in green, IHC signal transformed to red and the overlap of both signals in yellow to permit quantitative assessment of the signal overlap area (2c). The bottom row of images shows cortical FDDNP (green in 2d), IHC to tau (brown in 2e) and superimposed images of the two signals in 2f. High degree of signal overlap can be seen in FDDNP–PrP IHC superimposed images, while much less overlap is revealed by the superposition of FDDNP and tau IHC images. Size bar = 150 μm (1a–2c), 15 μm (2d–2f).

REFERENCES

1. Boxer A, Rabinovici G, Kepe V, Goldman J, Furst AJ, Huang S-C *et al* (2007) Amyloid imaging in distinguishing prion disease from Alzheimer disease. *Neurology* **69**:283–290.
2. Bresjanac M, Smid LM, Vovko TD, Petrič A, Barrio JR, Popovic M (2003) Molecular imaging probe 2-(1-{6-[(2-fluoroethyl)(methyl)amino]-2-naphthyl}ethylidene)-malononitrile labels prion plaques *in vitro*. *J Neurosci* **23**:8029–8033.
3. Collinge J (2001) Prion diseases of humans and animals: their causes and molecular basis. *Annu Rev Neurosci* **24**:519–550.
4. Collinge J (2005) Molecular neurology of prion disease. *J Neurol Neurosurg Psychiatry* **76**:906–919.
5. DeArmond SJ, Prusiner SB (1995) Etiology and pathogenesis of prion disease. *Am J Pathol* **146**:785–811.
6. DeArmond SJ, Prusiner SB (2003) Perspectives on prion biology, prion disease pathogenesis, and pharmacologic approaches to treatment. *Clin Lab Med* **23**:1–41.
7. Farlow MR, Yee RD, Dlouhy SR, Conneally PM, Azzarelli B, Ghetti B (1989) Gerstmann–Sträussler–Scheinker disease: I. Extending the clinical spectrum. *Neurology* **39**:1446–1452.
8. Gambetti P, Parchi P, Chen SG (2003) Herediatry Creutzfeldt–Jakob disease and fatal familial insomnia. *Clin Lab Med* **23**:43–64.
9. Ghetti B, Tagliavini F, Masters CL, Beyreuther K, Giaccone G, Verga L *et al* (1989) Gerstmann–Sträussler–Scheinker disease. II. Neurofibrillary tangles and plaques with PrP-amyloid coexist in an affected family. *Neurology* **39**:1453–1461.
10. Ghetti B, Tagliavini F, Takao M, Bugiani O, Piccardo P (2003) Hereditary prion protein amyloidosis. *Clin Lab Med* **23**:65–85.
11. Goldfarb LV, Brown P (1995) The transmissible spongiform encephalopathies. *Annu Rev Med* **47**:57–65.
12. Henkel K, Zerr I, Hertel A, Gratz KF, Schröter A, Tschampa HJ *et al* (2002) Positron emission tomography with [^{18}F]FDG in the diagnosis of Creutzfeldt–Jakob disease (CJD). *J Neurol* **249**:699–705.
13. Hsiao KK, Cass C, Schellenberg GD, Bird T, Devine-Gage E, Wisniewski H *et al* (1991) A prion protein variant in a family with the telencephalic form of Gerstmann–Sträussler–Scheinker syndrome. *Neurology* **41**:681–684.
14. Irisawa M, Amanuma M, Kozawa E, Kimura F, Araki N (2007) A case of Gerstmann–Sträussler–Scheinker syndrome. *Magn Reson Med Sci* **6**:53–57.
15. Ishikawa K, Doh-ura K, Kudo Y, Nishida N, Murakami-Kubo I, Ando Y *et al* (2004) Amyloid imaging probes are useful for detection of prion plaques and treatment of transmissible spongiform encephalopathies. *J Gen Virol* **85**:1785–1790.
16. Kepe V, Barrio JR, Huang S-C, Ercoli L, Siddarth P, Shoghi-Jadid K *et al* (2006) Serotonin 1A receptors in the living brain of Alzheimer's disease patients. *Proc Natl Acad Sci USA* **103**:702–707.
17. Klunk WE, Price JC, Mathis CA, Tsopelas ND, Lopresti BJ, Ziolko SK *et al* (2007) Amyloid deposition begins in the striatum of presenilin-1 mutation carriers from two unrelated pedigrees. *J Neurosci* **27**:6174–6184.
18. Lezak MD, Howieson D, Loring D (2004) *Neuropsychological Assessment*, 4th edn. Oxford University Press: New York.
19. Liu J, Kepe V, Žabjek A, Petrič A, Padgett HC, Satyamurthy N *et al* (2007) High-yield, automated radiosynthesis of 2-(1-{6-[(2-[^{18}F]fluoroethyl)(methyl)amino]-2-naphthyl}ethylidene)malononitrile ([^{18}F]FDDNP) ready for animal and human administration. *Mol Imaging Biol* **9**:6–16.
20. Logan J, Fowler J, Volkow N, Wang G, Ding YS, Alexoff DL (1996) Distribution volume ratios without blood sampling from graphical analysis of PET data. *J Cereb Blood Flow Metabol* **16**:834–840.
21. Mastrianni JA, Roos RP (2000) The prion diseases. *Semin Neurol* **20**:337–352.
22. Mazziotta JC, Phelps ME, Pahl JJ, Huang SC, Baxter LR, Riege WH *et al* (1987) Reduced cerebral glucose metabolism in asymptomatic subjects at risk for Huntington's disease. *N Engl J Med* **316**:357–362.
23. Molnár MJ, Valikovics A, Molnár S, Trón L, Diószeghy P, Mechler F *et al* (2000) Cerebral blood flow and glucose metabolism in mitochondrial disorders. *Neurology* **55**:544–548.
24. Padgett HC, Schmidt DG, Luxen A, Bida GT, Satyamurthy N, Barrio JR (1989) Computer-controlled radiochemical synthesis: a chemistry process control unit for the automated production of radiochemicals. *Int J Rad Appl Instrum A* **40**:433–445.
25. Parchi P, Gambetti P (1998) Human prion diseases. *Curr Opin Neurol* **8**:286–295.
26. Prusiner SB (1998) Prions. *Proc Natl Acad Sci USA* **95**:13363–13383.
27. Prusiner SB (2001) Shattuck lecture—neurodegenerative diseases and prions. *N Engl J Med* **344**:1516–1526.
28. Prusiner SB, Scott MR, DeArmond SJ, Cohen FE (1998) Prion protein biology. *Cell* **93**:337–348.
29. Sadowski M, Pankiewicz J, Scholtzova H, Tsai J, Li Y, Carp RI *et al* (2004) Targeting prion amyloid deposits *in vivo*. *J Neuropathol Exp Neurol* **63**:775–784.
30. Safar J, Roller PP, Gajdusek DC, Gibbs CJ Jr (1993) Conformational transitions, dissociation, and unfolding of scrapie amyloid (prion) protein. *J Biol Chem* **268**:20276–20284.
31. Small GW, Kepe V, Ercoli L, Siddarth P, Bookeheimer SY, Miller KJ *et al* (2006) PET of brain amyloid and tau in mild cognitive impairment. *N Engl J Med* **355**:2652–2663.
32. Smid LM, Vovko TD, Popovic M, Petrič A, Kepe V, Barrio JR *et al* (2006) The 2,6-disubstituted naphthalene derivative FDDNP labeling reliably predicts Congo red birefringence of protein deposits in brain sections of selected human neurodegenerative diseases. *Brain Pathol* **16**:124–130.

33. Taber KH, Cortelli P, Staffen W, Harley R (2002) The expanding role of imaging in prion disease. *J Neuropsychiatry Clin Neurosci* **14**:371–376.
34. Tanaka Y, Minematsu K, Moriyasu H, Yamaguchi T, Takenori Y, Kitamoto T *et al* (1997) A Japanese family with a variant of Gerstmann–Sträussler–Scheinker disease. *J Neurol Neurosurg Psychiatry* **62**:454–457.
35. Uchino A, Yoshinaga M, Shiokawa O, Hata H, Ohno M (1991) Serial MR imaging in Creutzfeldt–Jakob disease. *Neuroradiology* **33**:364–367.
36. Webb TE, Poulter M, Beck J, Uphill J, Adamson G, Campbell T *et al* (2008) Phenotypic heterogeneity and genetic modification of P102L inherited prion disease in an international series. *Brain* **131**:2632–2646.
37. Wong K-P, Kepe V, Small GW, Satyamurthy N, Barrio JR, Huang S-C (2007) Comparison of simplified methods for quantitative analysis of [^{18}F]FDDNP PET data. In: Conference Record, *2007 IEEE Nuclear Science Symposium and Medical Imaging Conference*, Honolulu, Hawaii, 2007, pp. 3146–3150.

SUPPORTING INFORMATION

Additional Supporting Information may be found in the online version of this article:

Figure S1. Correlation of [F-18]FDDNP Logan analysis approaches: white matter vs. cerebellum as reference region.
Figure S2. Coronal T1 magnetic resonance images. Evidence of ventricular dilation and atrophy.
Figure S3. [F-18]FDDNP DVR scatter plots for several cortical regions (A–E) and cerebellum (F).
Figure S4. Scatter plots for global (I) and regional cortical (A–E), striatal (G), thalamic (H) and cerebellar (F) [F-18]FDG SUVR values.
Figure S5. Scatter plots of [F-18]FDDNP R1 values in striatum (left) and thalamus (right).
Table S1. [F-18]FDDNP DVR *Z* scores in reference to the control group.
Table S2. [F-18]FDG SUVR *Z* scores in reference to the control group.
Table S3. Grading of clinical symptoms.
Table S4. Results of neuropsychological testing of Gerstmann–Sträussler–Scheinker subjects at the time of PET/MRI scans.

Please note: Wiley-Blackwell are not responsible for the content or functionality of any supporting materials supplied by the authors. Any queries (other than missing material) should be directed to the corresponding author for the article.